Linear stability of cylindrical Couette flow in the convection regime

Mohamed E. Ali[a)]
Department of Mechanical Engineering, King Saud University, P. O. Box 800, Riyadh 11421, Saudi Arabia

G. B. McFadden[b)]
National Institute of Standards and Technology, Gaithersburg, Maryland 20899-8910

The instability of steady circular Couette flow with radial heating across a vertically oriented annulus with a rotating inner cylinder and a stationary outer cylinder is investigated using a linear stability analysis. The convection regime base flow is developed for an infinite aspect ratio geometry and constant fluid properties with buoyancy included through the Boussinesq approximation. The base flow is characterized by a dimensionless stratification parameter γ that is proportional to the vertical temperature gradient. Critical stability boundaries are calculated for this assumed base flow with respect to both toroidal and helical disturbances. The numerical investigation is primarily restricted to a radius ratio of 0.6 at a Prandtl number of 100. Critical stability boundaries in Taylor–Grashof number space are presented for two values of the stratification parameter γ (4 and 13). The results follow the development of critical stability from Taylor cells at small Grashof numbers up to a maximum Grashof number used in this calculation of 20 000 and 80 000 for γ =4 and 13, respectively. Results show that increasing the stratification parameter stabilizes the isothermal Taylor vortices, followed by a destabilization at higher azimuthal mode numbers ($n > 0$). The results also show that for $\gamma=4$ (close to the conduction regime), two modes are obtained: one is axisymmetric and the other is nonaxisymmetric. However, for the convection regime (large γ) six asymmetric modes are obtained. Finally, the disturbance wavelength, phase speed, and spiral inclination angle are presented as a function of the critical Grashof number for the stratification parameters considered in this work. © *2005 American Institute of Physics.*
[DOI: 10.1063/1.1905482]

I. INTRODUCTION

The viscous fluid flow created between differentially rotating coaxial cylinders has provided a fertile testing ground for both linear and nonlinear stability theory. Beginning with the work of Taylor[1] numerous experimental and theoretical studies on flow transitions and morphologies of supercritical circular Couette flow have appeared. Initial studies on thermally driven circular Couette flow, motivated by technological problems in the cooling of rotating electrical machinery, have been reviewed by Kreith.[2] Early theoretical attacks neglected gravity and usually considered only axisymmetric disturbances in the limit of infinite aspect ratio. Such investigations by Yih,[3] Becker and Kaye,[4] Walowit *et al.*,[5] Bahl,[6] and Soundalgekar *et al.*[7] showed that isothermal Taylor cells are destabilized (stabilized) by positive (negative) radial heating gradients across the gap. Roesner[8] is credited as being the first to properly include the effect of gravity in the Boussinesq approximation but, like most of his predecessors, considered only axisymmetric disturbances. Roesner's results contrast those neglecting gravity in that isothermal Taylor cells are stabilized by both positive and negative radial heating and his computed stability boundaries exhibit perfect symmetry with respect to the direction of the temperature

gradient. There has been a renewed interest in the problem of radially heated rotating flows, partially from a continued effort to enhance the cooling of rotating machinery (Lee and Minkowyez[9]), but also with the aim of understanding and controlling instabilities in nematic liquid crystal systems (Barratt and Zuniga[10]) and in the solidification of pure metal (Vives[11]). Numerical studies of the effects of buoyancy on bifurcation phenomena in systems of small-to-moderate aspect ratio have been reported by Ball and Farouk.[12,13] Comprehensive studies on the stability of Taylor–Couette flow with radial heating using a conduction regime base flow have been conducted by Ali[14] and by Ali and Weidman[15] for both wide and narrow gaps and for different Prandtl numbers. Their results follow the development of critical stability from Taylor cells at zero heating through a number of asymmetric modes. Thermal convection in differentially rotating systems where the centrifugal force dominates over gravity was studied by Kropp and Busse.[16] Over a considerable range of the parameter space either convection rolls aligned with the axis of rotation or rolls in the azimuthal direction were found using the narrow gap approximation. The interaction of a small radial temperature gradient with both gravity and centrifugal forces was studied by Chen and Kuo[17] using a linear stability analysis. Their study showed that the symmetries found by Ali and Weidman[15] can be broken if the dependence of the centrifugal force on temperature gradient is included in the stability analysis. However, their analysis is

---

[a)]Telephone: 966-1-467-6672. Fax: 966-1-467-6652. Electronic mail: mali@ksu.edu.sa
[b)]Author to whom correspondence should be addressed. Telephone: 1-301-975-2711. Fax: 1-301-948-9720. Electronic mail: mcfadden@nist.gov

restricted to axisymmetric disturbances. On the other hand, the limiting case in which the centrifugal force is much smaller than the buoyancy force was studied by Auer *et al.*[18] using a small gap approximation. In their studies, both cylinders were rotating and linear stability analyses with some weakly nonlinear regimes were presented.

The stability of viscous isothermal circular Couette flow generated by rotation of the inner cylinder is controlled by the radius ratio, the aspect ratio, and the Taylor number. Stationary counterrotating toroidal cells of uniform width stacked one above the other appear at a critical Taylor number. Comprehensive reviews of both theory and experiments on the stability of isothermal circular Couette flow have been given by Di Prima and Swinney,[19] and Stuart.[20]

In the absence of rotation, natural convection between vertical differentially heated concentric cylinders depends crucially on the magnitude of the imposed thermal heating and the system aspect ratio $A=H/L$, where H is the annulus height and L is the gap width. Early experimental studies, starting by Eckert and Carlson,[21] fostered the identification of three distinct flow regimes in both planar and cylindrical gaps: conduction, transition, and convection. For circular cylinders maintained at different uniform temperatures, the transition regime for unity Prandtl number has been placed in the range of Rayleigh numbers,[22]

$$400A < \text{Ra} < 3000A \quad (A > 5),$$

where $\text{Ra} < 400A$ corresponds to the conduction regime and $\text{Ra} > 3000A$ to the convection regime where axial boundary layers form along each cylinder wall. In the limit $A \to \infty$, an analytical solution for the base flow in the conduction regime is readily obtained. A linearized Galekerin calculation testing the stability of this flow against axisymmetric disturbance has been carried out by Choi and Korpela.[23] McFadden *et al.*[24] extended Choi and Korpela's results by testing stability with respect to nonaxisymmetric disturbances. Weidman and Mehrdadtehranfar[25] have carried out experiments on the stability of natural convection in a vertical differentially heated annulus for base flows in the convection regime. They observed the simultaneous upward and downward propagation of vortex rings.

On the other hand, stability analyses of the convection regime in a planar gap have been carried out by Vest and Arpaci,[26] Gotoh and Mizushima,[27] Hart,[28] Elder,[29] and Bergholz.[30]

The purpose of this study is to develop an analytical solution for the base flow in the convection regime in a vertical annulus with a rotating inner cylinder and a stationary outer cylinder. Then the stability of this base flow is tested with respect to axisymmetric and asymmetric disturbances for a high Prandtl number ($\text{Pr}=100$) in a wide gap ($\kappa=0.6$). The mathematical formulation in Sec. II leads to the numerical solution procedure in Sec. III. Computed stability boundaries along with the associated disturbance wave characteristics are discussed in Sec. IV, followed by conclusions in Sec. V. The Appendix contains the analytical form of the base flow solution.

II. MATHEMATICAL FORMULATION

The motion of a thermally active viscous fluid in an annulus with a rotating inner cylinder and a stationary outer cylinder is governed by the equation of continuity, the Navier–Stokes equations, and the energy equation. The Boussinesq approximation is invoked for the buoyancy term, but otherwise constant fluid properties are presumed. To consider flow in the convective regime, we will consider a modified problem[30] in which the vertical temperature gradient β that develops in the core of the flow when the Grashof number becomes large,[29] is instead imposed *a priori* along the vertical boundaries. The annulus is then assumed to be infinite in vertical extent, with the effect of aspect ratio A entering implicitly through the value of β which is used to model the flow. For high Prandtl number flows in a vertical slot, Elder[29] found experimentally that the relation $2\beta=\Delta T/H$ holds to a good approximation if the Grashof number is large enough, where ΔT is the temperature difference across the annulus gap.

The equations of motion are made dimensionless by choosing the scales $[L,U,\Delta T,\rho_0 U v/L, L/U, \Omega_1 R_1]$ for the length, radial and vertical velocities, temperature, pressure, time, and azimuthal velocity, respectively. Here $U = g\beta\Delta TL^2/v$ is a characteristic velocity, the gap width is $L = R_2 - R_1$, g is the acceleration due to gravity, α is the thermal expansion coefficient, ρ_0 is the density, v is the kinematic viscosity, and Ω_1 is the rotation rate of the inner cylinder. The dimensionless equations in a cylindrical coordinate system are given by

$$G\left[\frac{\partial u}{\partial t} + (u \cdot \nabla)u - \frac{v^2 S^2}{r}\right] = -\frac{\partial p}{\partial r} + \nabla^2 u - \frac{2S}{r^2}\frac{\partial v}{\partial \phi} - \frac{u}{r^2}, \tag{1}$$

$$GS\left[\frac{\partial v}{\partial t} + (u \cdot \nabla)v + \frac{uv}{r}\right] = -\frac{1}{r}\frac{\partial p}{\partial \phi} + S\nabla^2 v + \frac{2}{r^2}\frac{\partial u}{\partial \phi} - \frac{Sv}{r^2}, \tag{2}$$

$$G\left[\frac{\partial w}{\partial t} + (u \cdot \nabla)w\right] = -\frac{\partial p}{\partial z} + \nabla^2 w + \theta, \tag{3}$$

$$G\left[\frac{\partial \theta}{\partial t} + u\frac{\partial \theta}{\partial r} + \frac{vS}{r}\frac{\partial \theta}{\partial \phi} + w\frac{\partial \theta}{\partial z}\right] = \frac{1}{\text{Pr}}\nabla^2 \theta, \tag{4}$$

$$\frac{\partial u}{\partial r} + \frac{u}{r} + \frac{S}{r}\frac{\partial v}{\partial \phi} + \frac{\partial w}{\partial z} = 0, \tag{5}$$

where

$$\nabla^2 = \frac{1}{r}\frac{\partial}{\partial r}\left(r\frac{\partial}{\partial r}\right) + \frac{1}{r^2}\frac{\partial^2}{\partial \phi^2} + \frac{\partial^2}{\partial z^2}, \tag{6}$$

$$(u \cdot \nabla) = u\frac{\partial}{\partial r} + \frac{Sv}{r}\frac{\partial}{\partial \phi} + w\frac{\partial}{\partial z}$$

for $\kappa/(1-\kappa) < r < 1/(1-\kappa)$, where u, v, and w are the velocity components in the r, ϕ, and z directions, θ is the dimen-

sionless temperature, and $\kappa=R_1/R_2$ is the radius ratio. The dimensionless parameters $G=g\alpha\Delta TL^3/\nu^2$ and $\text{Pr}=\nu/k$ appearing in the equations are the Grashof and Prandtl numbers, respectively, where k is the thermal diffusivity.

The swirl parameter $S=\Omega_1 R_1/U$ appears because of the difference in normalization between the azimuthal and meridional velocities. All computed stability results are presented in terms of the Taylor number $\text{Ta}=2\kappa^2\Omega_1^2 L^4/\nu^2(1-\kappa^2)$ in lieu of S.

A. The base flow

The base flow in the convection regime corresponds to a steady, axisymmetric motion with $u=0$, $v=V(r)$, $w=W(r)$, and $\theta=\tau z+\Theta(r)$, where $\tau=\beta L/\Delta T$ is the dimensionless vertical temperature gradient. Here capital letters for the velocities and temperature are used to signify the base flow conditions. Equations (1)–(5) reduce to

$$\frac{\partial p}{\partial r}=GS^2\frac{V^2}{r}, \tag{7}$$

$$\frac{d^2V}{dr^2}+\frac{1}{r}\frac{dV}{dr}-\frac{V}{r^2}=0, \tag{8}$$

$$\frac{\partial p}{\partial z}=\frac{d^2W}{dr^2}+\frac{1}{r}\frac{dW}{dr}+\Theta+\tau z, \tag{9}$$

$$WG\tau\,\text{Pr}=\frac{d^2\Theta}{dr^2}+\frac{1}{r}\frac{d\Theta}{dr}. \tag{10}$$

The pressure is then given by $p=p_0+Pz+\tau z^2/2$, where p_0 and P are constants. The vertical velocity thus satisfies

$$P=\frac{d^2W}{dr^2}+\frac{1}{r}\frac{dW}{dr}+\Theta. \tag{11}$$

We assume that W satisfies no-slip boundary conditions, and that $\Theta=1$ at $r=\kappa/(1-\kappa)$ and $\Theta=0$ at $r=1/(1-\kappa)$. The constant P is determined by requiring that there be no net mass flux in the axial direction:

$$0=\int_{\kappa/(1-\kappa)}^{1/(1-\kappa)}rW(r)dr. \tag{12}$$

The solution may be expressed in terms of Kelvin functions of order zero.[31] If we write $\tau\,\text{Pr}\,G=\gamma^4$, where γ is the stratification parameter, then we have

$$W(r)=a_1\,\text{ber}(\gamma r)+a_2\,\text{bei}(\gamma r)+a_3\,\text{ker}(\gamma r)+a_4\,\text{kei}(\gamma r), \tag{13}$$

and the temperature is given by

$$\Theta(r)=\gamma^2 a_1\,\text{bei}(\gamma r)-\gamma^2 a_2\,\text{ber}(\gamma r)+\gamma^2 a_3\,\text{kei}(\gamma r)$$
$$-\gamma^2 a_4\,\text{ker}(\gamma r)+P. \tag{14}$$

The coefficients a_1, a_2, a_3, and a_4 are given in the Appendix. The axial velocity and temperature profiles, $W(r)$ and $\Theta(r)$, are displayed in Figs. 1(a) and 1(b) for various values of γ
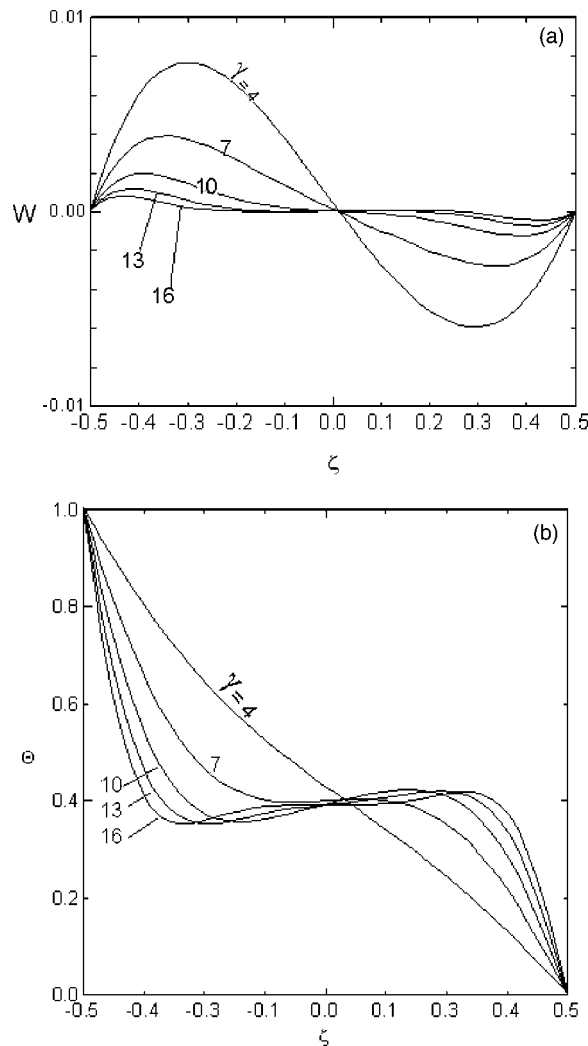
FIG. 1. Base flow for various values of the stratification parameter γ: (a) velocity and (b) temperature. Here the dimensionless temperature is $r=\kappa/(1-\kappa)+\zeta+1/2$.

ranging from 4 (close to conduction regime) to 16 (convection regime) and for $\kappa=0.6$. The base flow solutions can also be computed by using the two-point boundary value problem software SUPORT.[32] The numerical solutions were checked against the analytic formulas (13) and (14) using the IMSL software for the Kelvin functions. In the limit $\kappa\rightarrow 1$, the solutions approach those that are appropriate for a vertical planar slot.[30] The common solution for the azimuthal velocity in Eq. (8) is given by

$$V(r)=\frac{\kappa}{1+\kappa}\left[\frac{1}{(1-\kappa)^2 r}-r\right]. \tag{15}$$

B. The disturbance equations

The primitive variables are written as the sum of the base flow and a perturbed flow of the form

$$\begin{pmatrix} u(r,\phi,z,t) \\ v(r,\phi,z,t) \\ w(r,\phi,z,t) \\ p(r,\phi,z,t) \\ \theta(r,\phi,z,t) \end{pmatrix} = \begin{pmatrix} 0 \\ V(r) \\ W(r) \\ p_o + Pz + \tau z^2/2 \\ \tau z + \Theta(r) \end{pmatrix}$$

$$+ \begin{pmatrix} \hat{u}(r) \\ \hat{v}(r) \\ \hat{w}(r) \\ \hat{p}(r) \\ \hat{\theta}(r) \end{pmatrix} \exp[i(Kz - n\phi + \sigma_i t) + \sigma_r t].$$

$$(16)$$

In this formulation the disturbances are either toroidal ($n = 0$) or spiral ($n \neq 0$) with axial wavenumber K, frequency $-\sigma_i$, and growth rate σ_r. The radial eigenfunctions $\hat{u}(r), \hat{v}(r), \hat{w}(r), \hat{\theta}(r)$, and $\hat{p}(r)$ are complex quantities and for the determination of neutral stability, we set $\sigma_r = 0$. Substituting (16) into (1)–(5), subtracting the base flow and neglecting terms that are quadratic or higher in the perturbation amplitudes furnishes the linear stability governing equations,

$$D\hat{u} + \frac{\hat{u}}{r} + \frac{S}{r}in\hat{v} + iK\hat{w} = 0, \tag{17}$$

$$G(\sigma + iKW)\hat{u} + D\hat{p} = D^2\hat{u} + \frac{1}{r}D\hat{u} - \left[K^2 + \frac{(1+n^2)}{r^2}\right]\hat{u}$$

$$+ \frac{2inS}{r^2}\hat{v} + \frac{inGSV}{r}\hat{u} + \frac{2V\hat{v}}{r}S^2G, \tag{18}$$

$$G(\sigma + iKW)\hat{v} - \frac{in\hat{p}}{Sr} = D^2\hat{v} + \frac{1}{r}D\hat{v} - \left[K^2 + \frac{(1+n^2)}{r^2}\right]\hat{v}$$

$$- \frac{2in}{Sr^2}\hat{u} + \frac{inVGS}{r}\hat{v} + G\left[\frac{V}{r} + DV\right]\hat{u}, \tag{19}$$

$$G(\sigma + iKW)\hat{w} + G(DW)\hat{u} + iK\hat{p}$$

$$= D^2\hat{w} + \frac{1}{r}D\hat{w} - \left[K^2 + \frac{n^2}{r^2}\right]\hat{w} + \frac{inGSV}{r}\hat{w} + \hat{\theta}, \tag{20}$$

$$G\,\mathrm{Pr}(\sigma + iKW)\hat{\theta} + G\,\mathrm{Pr}(D\,\Theta)\hat{u}$$

$$= D^2\hat{\theta} + \frac{1}{r}D\,\hat{\theta} - \left[K^2 + \frac{n^2}{r^2}\right]\hat{\theta} + \frac{inSVG}{r}\mathrm{Pr}\,\hat{\theta} + \gamma^4\hat{w}, \tag{21}$$

where $D = d/dr$. Note that in Eq. (21) the stratification parameter γ has been substituted in place of the dimensionless vertical temperature gradient τ as an independent parameter of the problem. The choice is arbitrary, because γ and τ are related ($\tau\,\mathrm{Pr}\,G = \gamma^4$), and in the present paper γ is specified directly (see the work by Bergholz[30] and Hart[28]). These equations are to be solved with homogeneous boundary conditions at $r = \kappa/(1-\kappa)$ and $r = 1/(1-\kappa)$. The phase function $(Kz - n\phi + \sigma_i t)$ in (16) with critical solution values for n, K,

and σ_i completely determines the shape and kinematics of the disturbance flow patterns at neutral stability. In particular, the nondimensional axial phase speed C, the wavelength λ normal to lines of constant phase, and the inclination angle ψ of spiral cells with respect to the horizontal are given by

$$C = \frac{-\sigma_i}{K}, \quad \lambda = \frac{2\pi}{\Gamma}, \quad \psi = \tan^{-1}\left(\frac{n}{rK}\right),$$

$$\Gamma = \sqrt{(n^2/r^2 + K^2)}, \tag{22}$$

where Γ is the disturbance wavenumber normal to the lines of constant phase. Note that the wavelength and inclination angle for the asymmetric disturbances depend on the radial coordinate; for a given mode of instability, spiral wavelength (inclination) will be shorter (steeper) when observed at the inner wall than when observed at the outer wall (see the work by Ali and Weidman[15,33]).

III. NUMERICAL SOLUTION PROCEDURE

Equations (17)–(21) can be written as a set of 16 nonlinear first-order ordinary differential equations. This system was solved using the boundary-value problem software package SUPORT (Ref. 32) in combination with the nonlinear equation solver SNSQE.[34] Computations were performed in double precision. Extensive code testing of the SUPORT package with the SNSQE solver[35] has been previously reported by McFadden *et al.*,[36] Ali,[14] Ali and Weidman,[15,33] and recently by Ali *et al.*[37] The eigenvalue problem may be written in the implicit functional form

$$F(G, \mathrm{Ta}, \mathrm{Pr}, K, \sigma_i, n, \kappa, \gamma) = 0. \tag{23}$$

The parameters G, Pr, K, n, γ, and κ are usually fixed and solution of the ordinary differential equations is obtained by iteration on the eigenvalue pair (Ta, σ_i). At fixed mode number n, a search is conducted to find the minimum Taylor number over all wavenumber K, denoted here as Ta_n. Sample neutral curves for $\gamma = 4$ and for $n = 0$ and 1 are given in Figs. 2(a) and 2(b) for $\kappa = 0.6$ and for different Grashof numbers. Other sample curves corresponding to $\gamma = 13$ are shown in Fig. 3 for different values of azimuthal mode number and Grashof number. Critical conditions are then determined as the minimum Ta_n over all positive and negative values of n, and the critical values so obtained are denoted by Ta_c, G_c, K_c, and $(\sigma_i)_c$. Minimum values for Ta_c were determined by incrementing the wavenumber in steps $\Delta K = 0.001$ in the vicinity of the extremum in order to obtain a more precise determination of K_c. For the higher modes at large Grashof numbers the integrations were extremely sensitive to the initial guess for the eigenvalue pair.

The use of SUPORT (Ref. 32) in combination with a root finder such as SNSQE (Ref. 34) allows a very accurate determination of the eigenvalue pairs, at the expense of requiring good initial estimates for the eigenvalues. These estimates can be obtained by continuation from previous solutions, as we have done here. A popular alternative is to discretize the equations by finite difference or spectral methods, and determine the complex eigenvalue $\sigma = \sigma_r + i\sigma_i$ by solving a matrix eigenvalue problem. This is a robust approach that requires
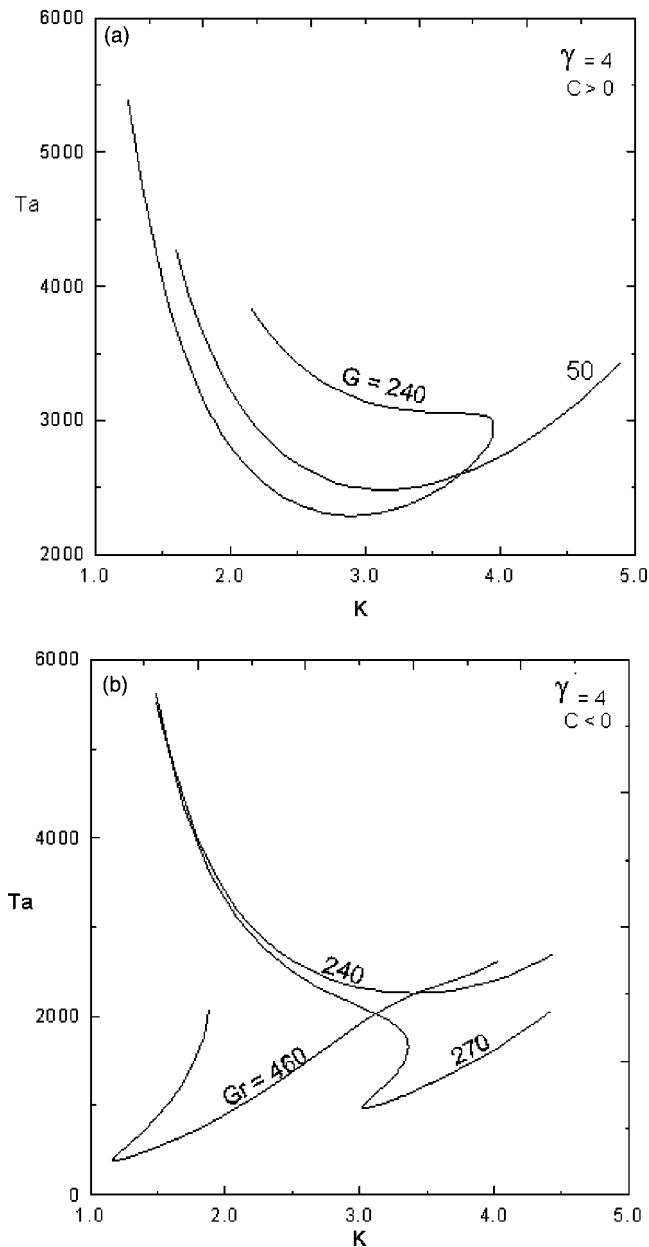
FIG. 2. Neutral stability curves for $\gamma=4$ and for various values of Grashof number for (a) axisymmetric mode ($n=0$) and (b) spiral mode ($n=1$).

FIG. 3. Samples of the neutral stability curves for different modes at various Grashof numbers for $\gamma=13$.

no initial guess, but the accuracy of the eigenfunction generally must be assessed by subsequent mesh refinement. In contrast, SUPORT is a spatially adaptive technique that is based on the use of local error estimates in the underlying ordinary differential equation solver to obtain solutions with specified accuracy.

IV. RESULTS AND DISCUSSION

The primary goal of this study is to track the evolution of the instability of steady circular Couette flow with radial heating in the convection regime from axisymmetric cells at small Grashof number through a range of nonaxisymmetric transitions with increasing G. Computations were carried out for $G>0$, Pr=100, wide gap ($\kappa=0.6$), and for two stratification parameter $\gamma=13$ and 4. Some general comments with respect to the overall results are given here. First, all critical conditions were found in the range $1.457 \leqslant \lambda_c \leqslant 2.365$ and these $O(1)$ values verify that the gap width L is the correct length scale for the problem, regardless of gap size or inclination angle of the spiral disturbances. Second, the critical spiral modes were always associated with positive values of n and σ_i corresponding to positive spiral inclination angle ψ and downward axial speed C. Third, the critical stability boundaries are searched for Grashof numbers up to 8×10^4 and 2×10^4 for $\gamma=13$ and 4, respectively. Finally, the axisymmetric modes always have two critical solutions associated with positive or negative σ_i corresponding to downward or upward drifting cells, respectively, and only the most unstable one is considered in the stability boundary.

In the present study we restrict out attention to the effect of buoyancy on the centrifugal instability of steady circular Couette flow at finite Taylor numbers. As an aside, we note that the stability of the base flow with radial heating but without rotation (Ta=0) is characterized by both shear and buoyant modes of instability. The shear modes are associated with the inflection point in the vertical velocity profile, and are relatively insensitive to Prandtl number. Critical Grashof numbers for the axisymmetric ($n=0$) shear mode for Ta=0, Pr=100, and $\kappa=0.6$ are 8378.5, 11 546.9, and 365 485 for $\gamma=0$, 4, and 13, respectively. The buoyant modes are associated with the extremes in the vertical velocity profile, and are prominent for large Prandtl numbers. For Ta=0, Pr=100, and $\kappa=0.6$ there are upward drifting ($\sigma_i<0$) axisymmetric modes with $G=643.02$, 703.67, and 4590.1 for $\gamma=0$, 4, and 13, respectively, and downward drifting ($\sigma_i>0$) axisymmetric modes with $G=968.79$, 1021.3, and 6478.5 for $\gamma=0$, 4, and 13, respectively. The effects of rotation on the shear and buoyant modes are outside the scope of this paper, and will be described in a separate publication.

The critical stability boundary separating stable from unstable circular Couette flow in Ta-G space for $\gamma=13$ is pre-
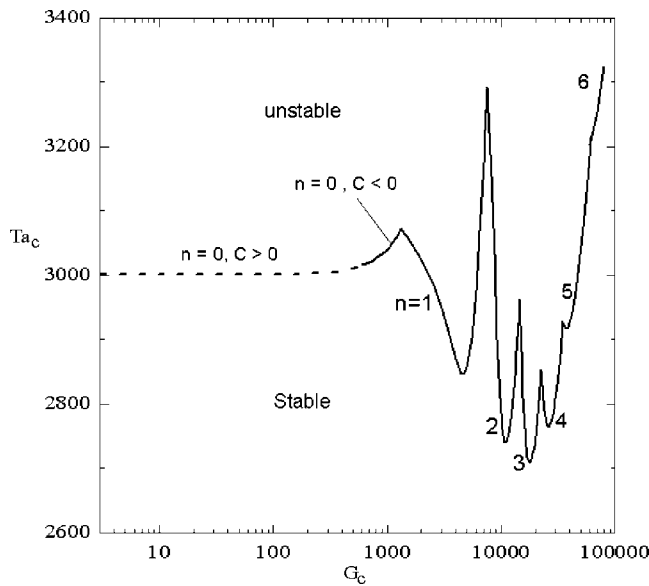
FIG. 4. Critical stability boundaries for $\gamma=13$ showing the flow bifurcation from the axisymmetric mode ($n=0$) to spiral modes $n>0$.
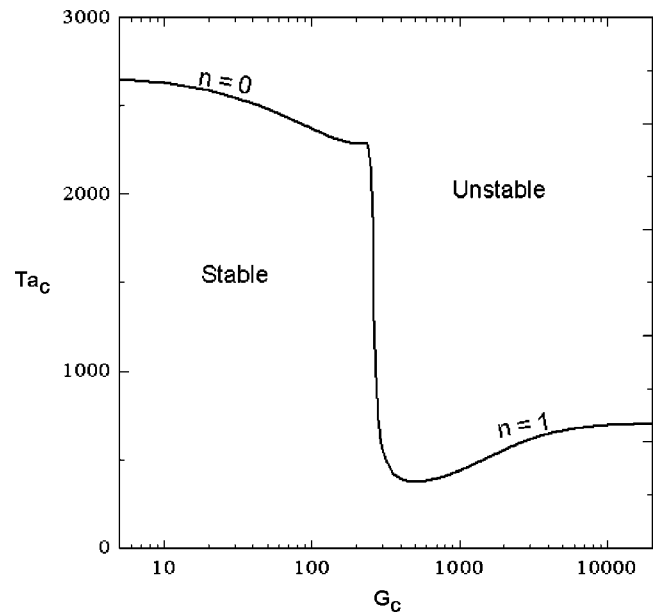
FIG. 5. Critical stability boundaries for $\gamma=4$ showing the flow bifurcation from the axisymmetric mode ($n=0$) to spiral mode $n=1$.

sented in linear-log form in Fig. 4. Increasing G stabilizes each axisymmetric mode up to the first onset of spiral instability. Note that dashed and solid lines for the $n=0$ mode correspond to cells drifting upward ($C>0$) and downward $C<0$, respectively. The critical curves progressively lose stability to spiral modes $n=1-6$ with increasing Grashof number. The critical Taylor and Grashof numbers at the intersection between the modes are given in Table I. Note also that as G increases n increases up to 3 where the flow is destabilized, and further increases in G tend to stabilize the flow with increasing n up to 6. On the other hand, the stability boundaries for $\gamma=4$ given in Fig. 5 exhibit strong destabilization of the axisymmetric mode. Here the critical curve bifurcates to spiral mode of $n=1$ only and the current search shows no evidence of higher modes up to $G=20\,000$. Observe that comparison between Figs. 4 and 5 shows that the effect of increasing the stratification parameter γ is to stabilize the flow. For example, at $n=0$ and $G=5$ the critical Taylor numbers are 2650.97 and 3001.08 for $\gamma=4$ and 13, respectively, which indicates that as γ tends to zero (conduction regime) at small Grashof numbers, Ta tends to the critical value of Taylor vortices Ta=2572.00.

The evolution of critical axial phase speeds, disturbance wavelengths, and spiral inclination angles along the stability boundary are given in Figs. 6–8, respectively. These figures compare two stratification parameter results for Pr=100 and $\kappa=0.6$. The values for λ_c and ψ_c were computed from Eq.

(22) at a radial position very near the outer cylindrical wall. Thus the spiral wavelengths and inclination angles are indicative of what one would observe from outside a transparent annulus using particle suspensions to visualize the flow (Weidman[38]) in a laboratory experiment. The axial phase speeds presented in Fig. 6 show that increasing the Grashof number reduces upward drift of the cells, but bifurcation to the spiral modes at higher Grashof number induces successively downward axial propagation speeds with weak discontinuities across each transition from $n=2$ up to 6 for $\gamma=13$ as shown in Fig. 6(a). However, the discontinuities are clear between $n=0$ and 1 for $\gamma=4$ [Fig. 6(b)]. Instability wavelengths presented in Fig. 7 change from $\lambda_c=1.822$ for weakly heated cells across the spiral modes to maximum values $\lambda_c=2.365$ for $\gamma=13$ and from $\lambda_c=1.985$ to 15.645 for $\gamma=4$. One observes, particularly for $\gamma=13$ in Fig. 7(a), that the wavelengths of successive helical modes grow continuously and then suddenly shrink to admit a new counterrotating cell pair into the annulus. Figure 8 shows the evolution of spiral inclination angle. At $\gamma=13$ the heated horizontal cells give way to spirals which tilt successively upward with the admission of each new helical wave; the terminal spiral mode angle is 55° as seen in Fig. 8(a). However, in Fig. 8(b) for $\gamma=4$ the terminal spiral mode angle is 85°, which is achieved for the first mode.

We conclude the discussion with a presentation of dis-

TABLE I. The critical points of Taylor and Grashof numbers at the intersection points between the different bifurcating modes for $\gamma=13$.

	$n=0$, $C>0$ $n=0$, $C<0$	$n=0$, $C<0$ $n=1$	$n=1$ $n=2$	$n=2$ $n=3$	$n=3$ $n=4$	$n=4$ $n=5$	$n=5$ $n=6$
Ta_c	3015	3071	3290	2 962	2 852	2 928	3 211
G_c	600	1325	7500	14 625	22 600	35 000	62 000
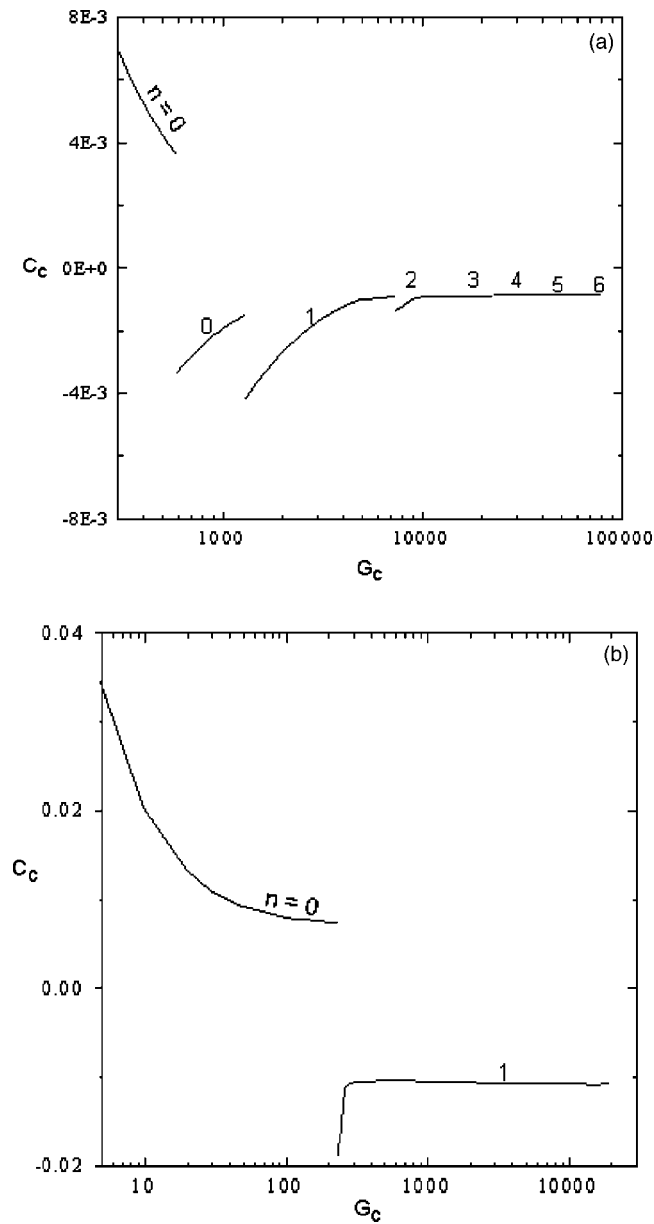
FIG. 6. A comparison of the evolution of vertical phase propagation speeds across (a) the six spiral modes for $\gamma=13$ and (b) the one spiral mode for $\gamma=4$.

turbance velocity vector fields and disturbance temperature contours. In Figs. 9 and 10 these fields are projected onto a meridional section over one vertical wavelength. In each frame the vertical wavelength has been scaled to a common height for ease of comparison. For the velocity vector fields portrayed in Fig. 9 the Grashof number increases from left to right following the evolution from approximate Taylor cells ($n=0$) through six examples of mixed convection to the asymmetric mode for $n=6$ shown in the final frame. The intervening spiral modes exhibit overlapping cells that are radially tilted outwards. Figure 10 shows the evolution of disturbance temperature contours exactly out of phase with their disturbance velocity counterparts in Fig. 9. The neatly stacked temperature cells in Fig. 10(a) for slightly heated flow become skewed and overlapping for the spiral modes with increasing n.
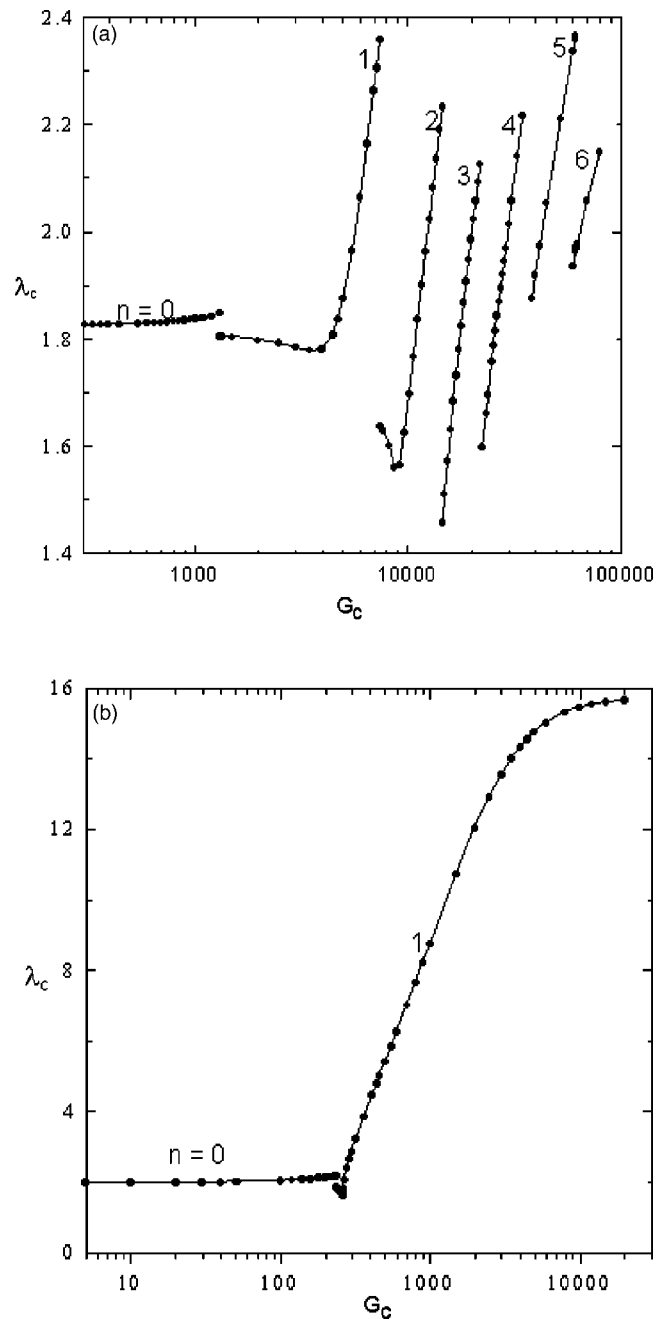
FIG. 7. A comparison of the evolution of wavelengths normal to the phase lines across (a) the six spiral modes for $\gamma=13$ and (b) the one spiral mode for $\gamma=4$.

V. CONCLUSIONS

The convection regime base flow has been derived and tested for different stratification parameters. The effect of this base flow on the stability of Taylor vortices has been determined for two stratification parameters $\gamma=4$ and 13, for a wide gap vertical annulus $\kappa=0.6$, and for $Pr=100$. The introduced stratification parameter γ tends to stabilize the Taylor vortices. However, for $\gamma=13$, as the Grashof number increases the stabilization effect continues through the axisymmetric mode only; destabilization occurs for $\gamma=4$ for the same mode. Furthermore, the axisymmetric modes always have two critical solutions, one corresponding to upward
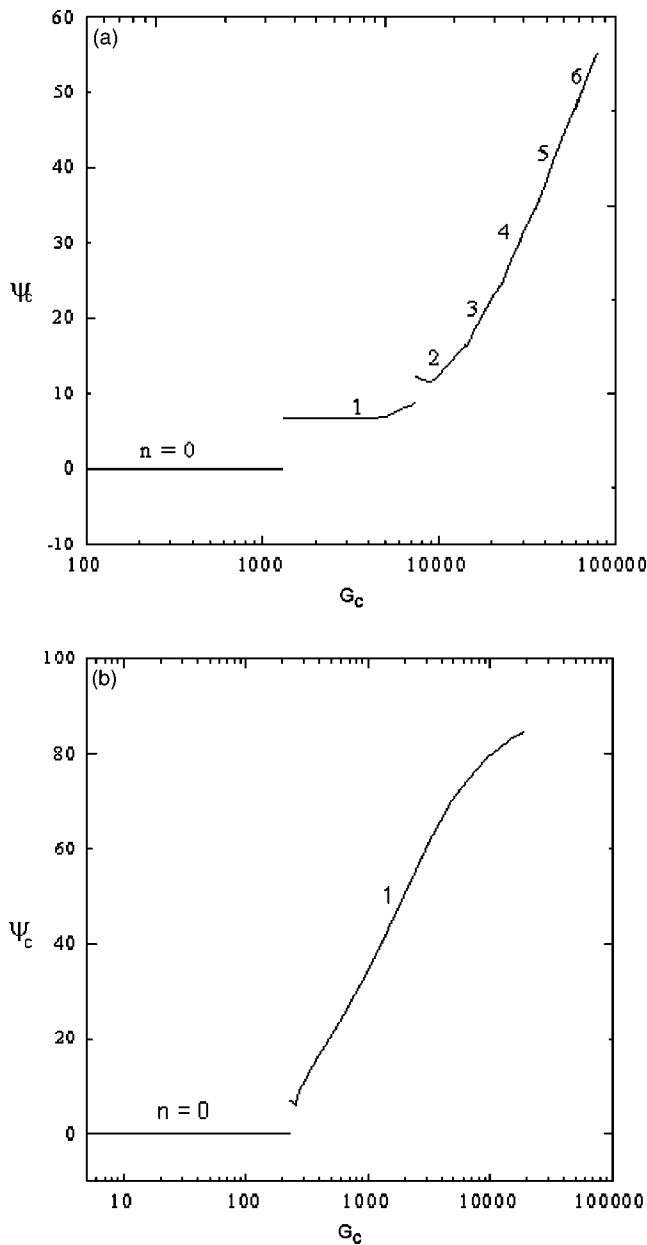
FIG. 8. A comparison of the evolution of spiral inclination angles across (a) the six spiral modes for $\gamma=13$ and (b) the one spiral mode for $\gamma=4$.

moving cells and the other to downward moving cells. The stability boundaries in Taylor–Grashof space are obtained and displayed in Figs. 4 and 5 for $\gamma=13$ and 4, respectively. For $\gamma=13$, six asymmetric modes are obtained where each mode starts with a destabilization effect followed by stabilization up to the intersection with the next higher mode in a spikelike shape directed downwards. This mechanism continues up to mode number 4. After that, only stabilization of the flow occurs. For $\gamma=4$, only two modes are found ($n=0,1$) with a destabilization influence throughout the region of Grashof number studied in this paper. Finally, as the mode numbers successively increase ($n=2$ and up for $\gamma=13$ and $n=1$ for $\gamma=4$) the terminal spiral phase speed becomes almost independent of the critical Grashof number.

ACKNOWLEDGMENTS

APPENDIX: THE BASE STATE

Here we give the coefficients for the velocity $W(r)$ and temperature $\Theta(r)$ in the base state. The velocity is given by

$$W(r) = a_1\,\mathrm{ber}(\gamma r) + a_2\,\mathrm{bei}(\gamma r) + a_3\,\mathrm{ker}(\gamma r) + a_4\,\mathrm{kei}(\gamma r),$$
(A1)

and the temperature is given by

$$\Theta(r) = \gamma^2 a_1\,\mathrm{bei}(\gamma r) - \gamma^2 a_2\,\mathrm{ber}(\gamma r) + \gamma^2 a_3\,\mathrm{kei}(\gamma r)$$
$$- \gamma^2 a_4\,\mathrm{ker}(\gamma r) + P.$$
(A2)

The (real-valued) Kelvin functions ber, bei, ker, and kei satisfy the equations,[31]

$$\left(D^2 + \frac{1}{r}D\right)\mathrm{ber}(\gamma r) + \gamma^2\,\mathrm{bei}(\gamma r) = 0,$$
(A3)

$$\left(D^2 + \frac{1}{r}D\right)\mathrm{bei}(\gamma r) - \gamma^2\,\mathrm{ber}(\gamma r) = 0,$$
(A4)

$$\left(D^2 + \frac{1}{r}D\right)\mathrm{ker}(\gamma r) + \gamma^2\,\mathrm{kei}(\gamma r) = 0,$$
(A5)

$$\left(D^2 + \frac{1}{r}D\right)\mathrm{kei}(\gamma r) - \gamma^2\,\mathrm{ker}(\gamma r) = 0,$$
(A6)

with $D \equiv d/dr$. Applying the boundary conditions

$$W(\kappa/\{1-\kappa\}) = W(1/\{1-\kappa\}) = \Theta(1/\{1-\kappa\}) = 0,$$

$$\Theta(\kappa/\{1-\kappa\}) = 1,$$

we obtain the linear system

$$\begin{pmatrix} \mathrm{ber}(\xi_1) & \mathrm{bei}(\xi_1) & \mathrm{ker}(\xi_1) & \mathrm{kei}(\xi_1) \\ \mathrm{bei}(\xi_1) & -\mathrm{ber}(\xi_1) & \mathrm{kei}(\xi_1) & -\mathrm{ker}(\xi_1) \\ \mathrm{ber}(\xi_2) & \mathrm{bei}(\xi_2) & \mathrm{ker}(\xi_2) & \mathrm{kei}(\xi_2) \\ \mathrm{bei}(\xi_2) & -\mathrm{ber}(\xi_2) & \mathrm{kei}(\xi_2) & -\mathrm{ker}(\xi_2) \end{pmatrix} \begin{pmatrix} a_1 \\ a_2 \\ a_3 \\ a_4 \end{pmatrix}$$
$$= \begin{pmatrix} 0 \\ \{1-P\}/\gamma^2 \\ 0 \\ -P/\gamma^2 \end{pmatrix},$$
(A7)

where $\xi_1 = \gamma\kappa/(1-\kappa)$ and $\xi_2 = \gamma/(1-\kappa)$. The solution to the linear system can be expressed in terms of the coefficients,

$$A_{rr} = \mathrm{ber}(\xi_1)\mathrm{ker}(\xi_2) - \mathrm{ber}(\xi_2)\mathrm{ker}(\xi_1),$$

$$A_{ir} = \mathrm{bei}(\xi_1)\mathrm{ker}(\xi_2) - \mathrm{bei}(\xi_2)\mathrm{ker}(\xi_1),$$

$$A_{ri} = \mathrm{ber}(\xi_1)\mathrm{kei}(\xi_2) - \mathrm{ber}(\xi_2)\mathrm{kei}(\xi_1),$$
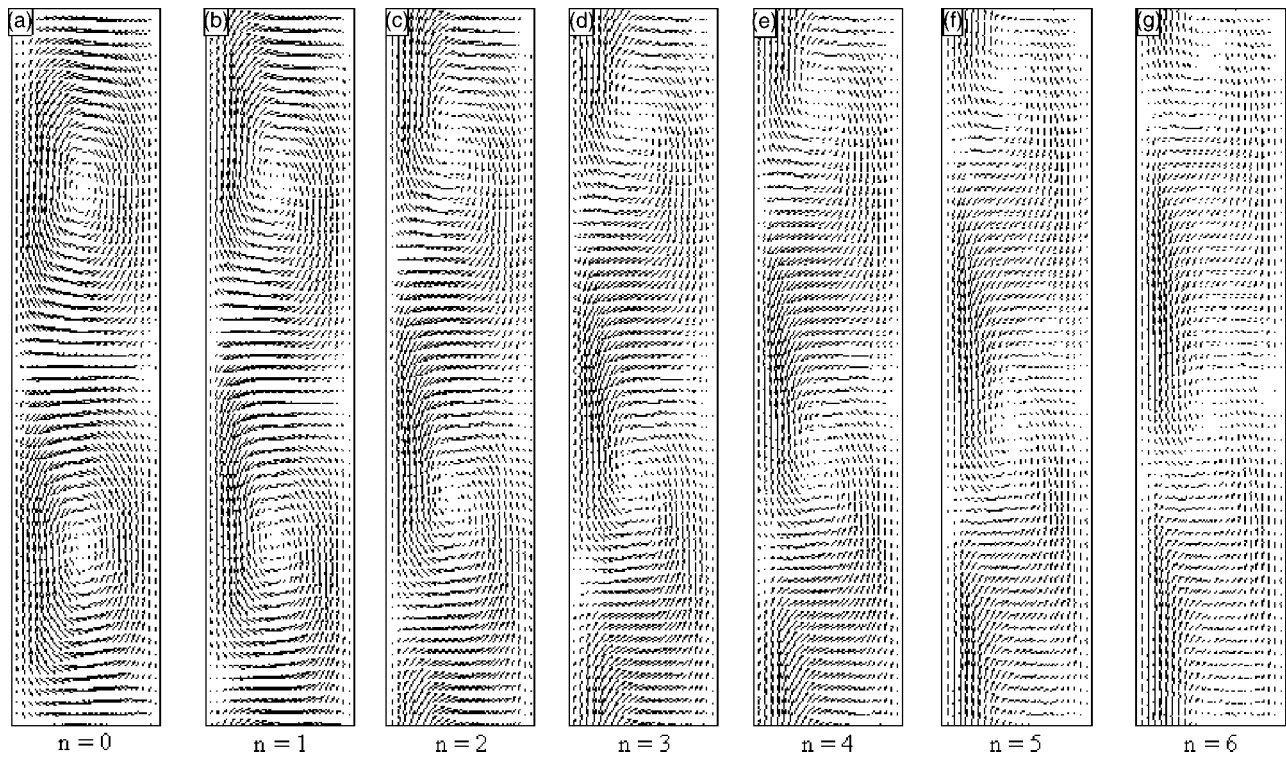
FIG. 9. Evolution of the disturbance velocity vector fields in a meridional section. The left wall of each figure locates the outer cylinder. Vertical wavelengths have been scaled to equal height. The actual wavelengths can be computed from the critical conditions: (a) $Ta_c=3001$, $G_c=3$, $K_c=3.45$; (b) $Ta_c=2847$, $G_c=4500$, $K_c=3.456$; (c) $Ta_c=2740$, $G_c=11\,220$, $K_c=3.33$; (d) $Ta_c=2709$, $G_c=18\,000$, $K_c=3.23$; (e) $Ta_c=2764$, $G_c=26\,000$, $K_c=3.071$; (f) $Ta_c=2974$, $G_c=45\,000$, $K_c=2.32$; (g) $Ta_c=3253$, $G_c=70\,000$, $K_c=1.89$.

$$A_{ii} = \mathrm{bei}(\xi_1)\mathrm{kei}(\xi_2) - \mathrm{bei}(\xi_2)\mathrm{kei}(\xi_1).$$

The determinant D of the linear system reduces to

$$D = A_{ri}^2 + A_{rr}^2 + A_{ii}^2 + A_{ir}^2 - 2[\mathrm{ber}(\xi_1)\mathrm{bei}(\xi_2) - \mathrm{ber}(\xi_2)\mathrm{bei}(\xi_1)][\mathrm{ker}(\xi_1)\mathrm{kei}(\xi_2) - \mathrm{ker}(\xi_2)\mathrm{kei}(\xi_1)],$$

$$(A8)$$

and the solution is given by

$$\gamma^2 D a_1 = P([\mathrm{ker}(\xi_2) - \mathrm{ker}(\xi_1)][A_{ir} - A_{ri}] + [\mathrm{kei}(\xi_2) - \mathrm{kei}(\xi_1)][A_{rr} - A_{ii}]) + \mathrm{kei}(\xi_2)[A_{ii} - A_{rr}] + \mathrm{ker}(\xi_2)[A_{ri} - A_{ir}],$$

$$(A9)$$
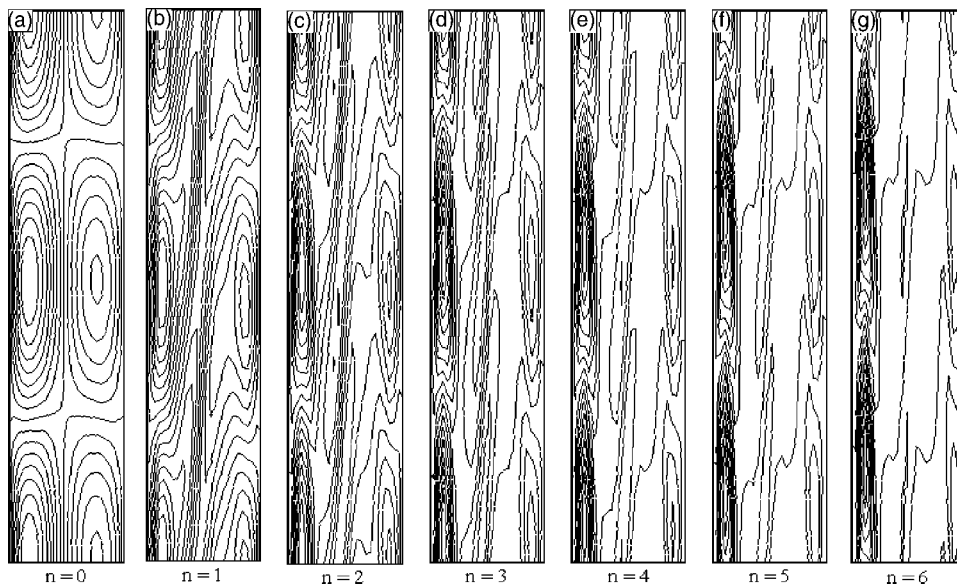
FIG. 10. Evolution of the disturbance temperature contours in a meridional section. See caption of Fig. 9 for critical conditions.

$$\gamma^2 Da_2 = P([\ker(\xi_2) - \ker(\xi_1)][-A_{rr} - A_{ii}] + [\text{kei}(\xi_2) - \text{kei}(\xi_1)][A_{ir} + A_{ri}]) + \text{kei}(\xi_2)[-A_{ir} - A_{ri}] + \ker(\xi_2)[A_{rr} + A_{ii}],$$ (A10)

$$\gamma^2 Da_3 = P([\text{ber}(\xi_2) - \text{ber}(\xi_1)][-A_{ir} + A_{ri}] + [\text{bei}(\xi_2) - \text{bei}(\xi_1)][A_{rr} + A_{ii}]) + \text{bei}(\xi_2)[-A_{ii} - A_{rr}] + \text{ber}(\xi_2)[A_{ir} - A_{ri}],$$ (A11)

$$\gamma^2 Da_4 = P([\text{ber}(\xi_2) - \text{ber}(\xi_1)][A_{ii} - A_{rr}] + [\text{bei}(\xi_2) - \text{bei}(\xi_1)][-A_{ir} - A_{ri}]) + \text{bei}(\xi_2)[A_{ir} + A_{ri}] + \text{ber}(\xi_2)[A_{rr} - A_{ii}].$$ (A12)

From the representation (A1) for W, we then find

$$\int_{\kappa/(1-\kappa)}^{1/(1-\kappa)} rW(r)dr = a_1 I_1 + a_2 I_2 + a_3 I_3 + a_4 I_4,$$ (A13)

where[31]

$$I_1 = \int_{\kappa/(1-\kappa)}^{1/(1-\kappa)} r\,\text{ber}(\gamma r)dr = \left. \frac{-\xi}{\sqrt{2}\gamma^2}[\text{ber}_1(\xi) - \text{bei}_1(\xi)]\right|_{\xi=\xi_1}^{\xi=\xi_2},$$ (A14)

$$I_2 = \int_{\kappa/(1-\kappa)}^{1/(1-\kappa)} r\,\text{bei}(\gamma r)dr = \left. \frac{-\xi}{\sqrt{2}\gamma^2}[\text{bei}_1(\xi) + \text{ber}_1(\xi)]\right|_{\xi=\xi_1}^{\xi=\xi_2},$$ (A15)

$$I_3 = \int_{\kappa/(1-\kappa)}^{1/(1-\kappa)} r\,\ker(\gamma r)dr = \left. \frac{-\xi}{\sqrt{2}\gamma^2}[\ker_1(\xi) - \text{kei}_1(\xi)]\right|_{\xi=\xi_1}^{\xi=\xi_2},$$ (A16)

$$I_4 = \int_{\kappa/(1-\kappa)}^{1/(1-\kappa)} r\,\text{kei}(\gamma r)dr = \left. \frac{-\xi}{\sqrt{2}\gamma^2}[\text{kei}_1(\xi) + \ker_1(\xi)]\right|_{\xi=\xi_1}^{\xi=\xi_2}.$$ (A17)

Setting the flux equal to zero in Eq. (A13) then gives a linear equation for P, which completes the solution of the base flow.

[1] G. I. Taylor, "Stability of a viscous liquid contained between two rotating cylinders," Philos. Trans. R. Soc. London, Ser. A **223**, 289 (1923).

[2] F. Kreith, "Convection heat transfer in rotating systems," Adv. Heat Transfer **5**, 129 (1968).

[3] C. S. Yih, "Dual role of viscosity in the stability of revolving fluids of variable density," Phys. Fluids **4**, 806 (1961).

[4] K. M. Becker and J. Kaye, "The influence of a radial temperature gradient on the instability of fluid flow in an annulus with an inner rotating cylinder," Trans. ASME, Ser. C: J. Heat Transfer **84**, 106 (1962).

[5] J. Walowit, S. Taso, and R. C. Di Prima, "Stability of flow between arbitrarily spaced concentric cylinder surfaces, including the effect of a radial temperature gradient," ASME Trans. J. Appl. Mech. **31**, 585 (1964).

[6] S. K. Bahl, "The effect of radial temperature gradient on the stability of a viscous flow between two rotating coaxial cylinders," ASME Trans. J. Appl. Mech. **39**, 593 (1972).

[7] V. M. Soundalgekar, H. S. Takhar, and J. T. Smith, "Effects of radial temperature gradient on the stability of viscous flow in an annulus with a rotating inner cylinder," Waerme-Stoffuebertrag. **15**, 233 (1981).

[8] K. G. Roesner, "Hydrodynamic stability of cylindrical Couette flow," Arch. Mech. **30**, 619 (1978).

[9] Y. N. Lee and W. J. Minkowycz, "Heat transfer characteristics of the annulus of two-coaxial cylinders with one cylinder rotating," Int. J. Heat Mass Transfer **32**, 711 (1989).

[10] P. J. Barratt and I. Zuniga, "A theoretical investigation of Benard–Couette instabilities in nematic liquid crystals," J. Phys. D **17**, 775 (1984).

[11] C. Vives, "Effects of a forced Couette flow during the controlled solidification of a pure metal," Int. J. Heat Mass Transfer **33**, 2047 (1988).

[12] S. K. Ball and B. Farouk, "On the development of Taylor vortices in a vertical annulus with a heated rotating inner cylinder," Int. J. Numer. Methods Fluids **7**, 857 (1987).

[13] S. K. Ball and B. Farouk, "Bifurcation and phenomena in Taylor–Couette flow with buoyancy effects," J. Fluid Mech. **197**, 479 (1988).

[14] M. E. Ali, "The stability of Taylor–Couette flow with radial heating," Ph.D. thesis, University of Colorado, Boulder, 1988.

[15] M. Ali and P. D. Weidman, "On the stability of circular Couette flow with radial heating," J. Fluid Mech. **220**, 53 (1990).

[16] M. Kropp and H. Busse, "Thermal convection in differentially rotating systems," Geophys. Astrophys. Fluid Dyn. **61**, 127 (1991).

[17] J. Chen and J. Kuo, "The linear stability of steady circular Couette flow with a small radial temperature gradient," Phys. Fluids A **2**, 1585 (1990).

[18] M. Auer, F. H. Busse, and E. Gangler, "Instabilities of flows between differentially rotating coaxial vertical cylinders in the presence of a radial temperature gradient," Eur. J. Mech. B/Fluids **15**, 605 (1996).

[19] R. C. Di Prima and H. L. Swinney, "Instabilities and transition in flow between concentric rotating cylinders," in *Hydrodynamic Instabilities and the Transition to Turbulence*, Topics in Applied Physics Vol. 45, edited by H. L. Swinney and J. P. Gollub (Springer, New York, 1981), pp. 139–180.

[20] J. T. Stuart, "Taylor vortex flow: a dynamical system," SIAM Rev. **28**, 315 (1986).

[21] E. R. G. Eckert and W. O. Carlson, "Natural convection in an air layer enclosed between two vertical plates with different temperatures," Int. J. Heat Mass Transfer **2**, 106 (1961).

[22] Based on numerical calculations by R. W. Thomas and G. de Vahl Davis in 1970, see the discussion in Ref. 25.

[23] I. G. Choi and S. A. Korpela, "Stability of the conduction regime of natural convection in a tall vertical annulus," J. Fluid Mech. **99**, 725 (1980).

[24] G. B. McFadden, S. R. Coriell, R. F. Boisvert, and M. E. Glicksman, "Asymmetric instabilities in a buoyancy-driven flow in a tall vertical annulus," Phys. Fluids **27**, 1359 (1984).

[25] P. D. Weidman and G. Mehrdadtehranfar, "Instability of natural convection in a tall vertical annulus," Phys. Fluids **28**, 776 (1985).

[26] C. M. Vest and V. S. Arpaci, "Stability of natural convection in a vertical slot," J. Fluid Mech. **36**, 1 (1969).

[27] K. Gotoh and J. Mizushima, "The stability of convection between two parallel vertical walls," J. Phys. Soc. Jpn. **34**, 1408 (1973).

[28] J. E. Hart, "Stability of the flow in a differentially heated inclined box," J. Fluid Mech. **47**, 547 (1971).

[29] J. W. Elder, "Laminar free convection in a vertical slot," J. Fluid Mech. **23**, 77 (1965).

[30] R. F. Bergholz, "Instability of steady natural convection in a vertical fluid layer," J. Fluid Mech. **84**, 743 (1978).

[31] *Handbook of Mathematical Functions with Formulas, Graphs, and Mathematical Tables*, Natl. Bur. Stand. Appl. Math. Ser. No. 55, edited by M. Abramowitz and I. A. Stegun (U.S. GPO, Washington, D.C., 1964), p. 379.

[32] M. R. Scott and H. A. Watts, "Computational solution of linear 2-point boundary-value problems via orthonormalization," SIAM (Soc. Ind. Appl. Math.) J. Numer. Anal. **14**, 40 (1977).

[33] M. E. Ali and P. D. Weidman, "On the linear stability of cellular spiral Couette flow," Phys. Fluids A **5**, 1188 (1993).

[34] SNSQE was written by K. L. Hiebert (1980), based on Powell (Ref. 35), and is part of the SLATEC Common Math Library. SLATEC is available from the NETLIB repository at the URL http://www.netlib.org/

[35] M. J. D. Powell, "A hybrid method for nonlinear equations," in *Numerical Methods for Nonlinear Algebraic Equations*, edited by P. Rabinowitz

(Gordon and Breach, New York, 1970), pp. 87–161.

[36]G. B. McFadden, S. R. Coriell, R. F. Boisvert, M. E. Glicksman, and Q. T. Fang, "Morphological stability in the presence of fluid flow in the melt," Metall. Trans. A **15A**, 2117 (1984).

[37]M. E. Ali, D. Mitra, J. A. Schwille, and R. M. Lueptow, "Hydrodynamic stability of suspension in cylindrical Couette flow," Phys. Fluids **14**, 1 (2002).

[38]P. D. Weidman, "Experimental techniques in laboratory rotating flows," in *Advances in Fluid Mechanics Measurements*, Lecture Notes in Engineering Vol. 45, edited by M. Gad-El-Hak (Springer, Berlin, 1989).